Feature Extraction of Separation and Attachment Lines

David N. Kenwright, *Member, IEEE*, Chris Henze, and Creon Levit

Abstract—Separation and attachment lines are topologically significant curves that exist on 2D surfaces in 3D vector fields. Two algorithms are presented, one point-based and one element-based, that extract separation and attachment lines using eigenvalue analysis of a locally linear function. Unlike prior techniques based on piecewise numerical integration, these algorithms use robust analytical tests that can be applied independently to any point in a vector field. The feature extraction is fully automatic and suited to the analysis of large-scale numerical simulations. The strengths and weaknesses of the two algorithms are evaluated using analytic vector fields and also results from computational fluid dynamics (CFD) simulations. We show that both algorithms detect open separation lines—a type of separation that is not captured by conventional vector field topology algorithms.

Index Terms—Vector field visualization, vector field topology, flow visualizaiton, feature detection, flow separation, separation line.

1 Introduction

Identifying regions of separated airflow is very important in the design of aircraft because flow separation can reduce lift and cause control problems when flying at slow speeds. Flow separation and attachment is said to occur when the flow abruptly leaves or returns to a solid body, as depicted in Fig. 1. It frequently occurs on the wings of aircraft when they are inclined relative to the onset airflow. This phenomenon has been studied for more than 50 years [5], [15], [22], [27] although there is still no consensus on a mathematical definition for separation in a 3D vector field, (discussed in Section 2).

A separated airflow causes a significant increase in drag and raises the stall speed of an aircraft—conditions that are particularly dangerous at takeoff and landing. In some aircraft, such as the delta wing shown in Fig. 1, flow separation and attachment must occur in order for the wings to produce lift. Fighter aircraft can also exploit separation to enable them to rapidly decelerate during a dogfight. The ability to predict when and where flow separation occurs in numerical simulations is clearly beneficial to aircraft designers because it helps them to predict flight characteristics before building or flying the prototype aircraft.

Separation and attachment lines and surfaces, though sometimes known by other names, are important not only in fluid dynamics but also in other fields of science. For example, Bader [1] and his colleagues have explained many features of molecular physics and quantum chemistry using the techniques of vector field topology. In their theory of "atoms in molecules," interatomic surfaces, i.e., boundaries between atoms in real space, are defined to be separation surfaces in the gradient of the electronic charge density.

- *D.N. Kenwright and C. Henze are with MRJ Technology Solutions, Inc., NASA Ames Research Center, Moffett Field, CA 94035. E-mail: {davidk, chenze}@nas.nasa.gov.*
- *C. Levit is with the National Aeronautics and Space Administration, NASA Ames Research Center, Moffett Field, CA 94035. E-mail: creon@nas.nasa.gov.*

For information on obtaining reprints of this article, please send e-mail to: tvcg@computer.org, and reference IEEECS Log Number 109334.

Two automatic feature extraction techniques will be described that locate and distinguish separation and attachment lines on solid bodies in 3D numerical flow fields. The algorithms are based on eigenvalue analysis of the velocity gradient tensor and perform a local analysis of the vector field rather than a global analysis of the entire flow field. They are useful for analyzing large partitioned data sets, such as those computed on distributed memory architectures, because the elements can be processed in parallel. Fully automated feature extraction techniques are increasingly necessary to analyze and extract information from the results of large-scale numerical simulations. Automated techniques have several advantages over traditional interactive visualization techniques. First, they eliminate the need for scientists or engineers to manually explore their data to find the features of interest. Second, the analysis can be done off-line on computers without graphics capability, such as the supercomputers that generate the data. Third, the feature extraction algorithms output 3D graphics primitives whose combined size is typically several orders of magnitude smaller than the original data set. This is a significant data reduction and enables the results to be interactively viewed on modest graphics workstations. Fourth, they provide quantitative information, e.g., the location of a separation line, which can be used to assess the effect of design modifications.

The contents of this paper are organized as follows. The various definitions for a separation line are discussed in Section 2. Prior techniques used to detect and visualize flow separation and attachment lines are discussed in Section 3. The mathematical foundations for the element- and point-based algorithms are presented in Sections 4 and 5. The algorithms are tested using analytic functions and CFD data in Section 6, and the results compared to those produced by particle tracing, line integral convolution, and flow topology algorithms on the same data sets. Section 7 gives an analysis, while Section 8 concludes this paper.

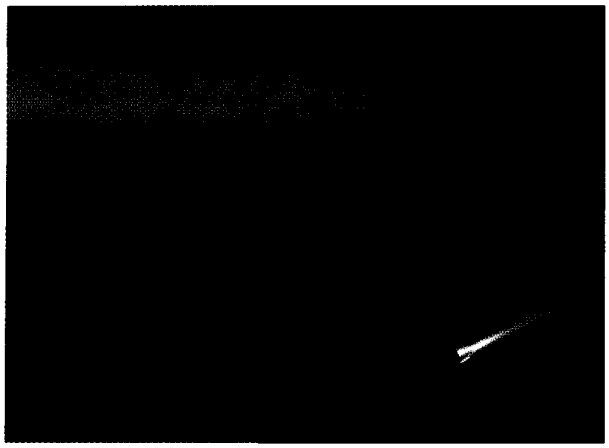

Fig. 1. Flow separation and attachment occurs along the edge of this delta wing aircraft where the airflow abruptly leaves and then returns to the surface. The curves along which this occurs are called separation and attachment lines.

2 Definition of a Separation Line

Separation is almost always studied in viscous flows, where the velocity field goes smoothly to zero on all solid surfaces ("no-slip boundary conditions"). In these cases, if one is interested in surface flow, one usually deals with *limiting streamlines*, which are streamlines in the wall shear stress vector field. The wall shear stress is defined as the normal derivative to the surface of the velocity vector field. Integral curves in this vector field are sometimes referred to as surface streamlines, wall shear-stress trajectories, or skin friction lines. It is this vector field which produces oil-flow patterns in wind tunnel experiments [16].

We can find no precise definition, mathematical or otherwise, of separation in 3D flows in the fluid dynamics or aeronautics literature. The common theme running through most descriptions of separation concerns flow turning away from a surface where it had been moving tangentially. In 2D flows, this can occur only at critical points (half-saddles) located on 1D boundaries. These critical points are just places where flows along the surface in opposing directions converge and, by continuity, the *wall shear stress is zero*. In fully 3D flows over a 2D boundary, there are 1D loci where flows in relatively opposing directions meet, but the criterion of zero wall shear stress does not generally hold, because there is almost always flow **along** the 1D curve. In fact, the wall shear stress can reach zero only at isolated points along these so-called "lines of separation."

Since streamlines cannot meet, except at critical points, flow converging from relatively opposing directions must turn and approach a separation line tangentially. This behavior has led some to characterizing separation lines as *streamline asymptotes* [24], [25], or *envelopes of streamlines* [26]. A more straightforward description is provided by Panton [18], who states simply: "Separation lines are lines on the surface where surface streamlines tend to accumulate."

3 Prior Work

Techniques used to identify separation and attachment lines in numerical flow simulations fall into one of two categories: phenomenological or topological. With phenomenological techniques, scientists must observe flow patterns on a surface and use their insight or experience to identify the separation and attachment lines. These techniques usually mimic flow visualization techniques used in wind and water tunnel experiments. The topological techniques are based on the mathematics of Poincare and identify specific features that originate from critical points.

3.1 Skin Friction Lines

Surface streamlines or skin friction lines are widely used phenomenological techniques [17]. The approach is to seed particles near a body and to compute integral curves (streamlines) that are constrained to the body. This approach can be effective if large numbers of particles are released because the curves merge together along separation lines, as shown in Fig. 2. Attachment lines are not usually so obvious because the particle paths diverge.

Because this approach relies on observation, the analyst must study the flow patterns to determine which lines correspond to separation and which to attachment. Both are visually similar, although it can usually be determined by examining the direction of the asymptotes in relation to the direction of the onset flow. The asymptotes generally curve downstream along separation lines and upstream along attachment lines. However, it becomes difficult to make the same distinction when the separation lines are perpendicular to the onset flow. Of greater concern is the amount of redundant information (i.e., irrelevant curves) that is generated by this technique.

3.2 Texture Synthesis

Texture synthesis techniques such as Line Integral Convolution (LIC) [3] and Spot Noise [23] create continuously shaded images that can effectively show the global structure of a flow. They have been applied to skin friction vector fields in CFD data sets [9], [10], [21] to create flow patterns that are strikingly similar to experimental visualizations. Fig. 3 shows the skin friction lines on the delta wing rendered using a LIC algorithm. Once again, this is a phenomenological technique that requires careful analysis to identify and distinguish separation and attachment lines in the flow patterns. This is relatively easy in steady-state

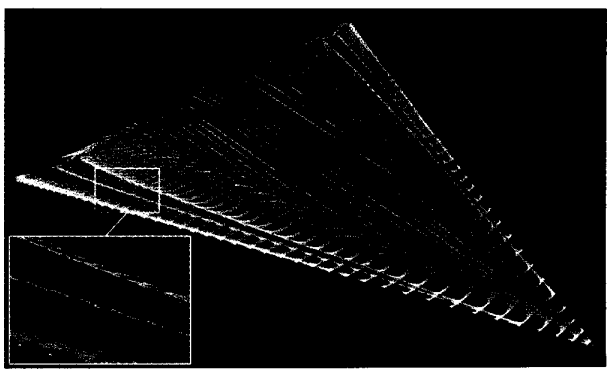

Fig. 2. The skin friction lines on the surface of the delta wing asymptotically approach separation lines and asymptotically leave attachment lines.

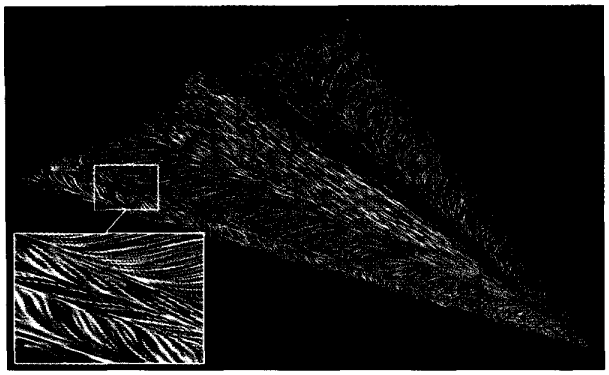

Fig. 3. A global surface flow visualization created using an LIC algorithm. The close-up (inset) reveals several parallel separation and attachment lines in close proximity, although the analyst must carefully study the direction of the asymptotes in order to distinguish one from the other.

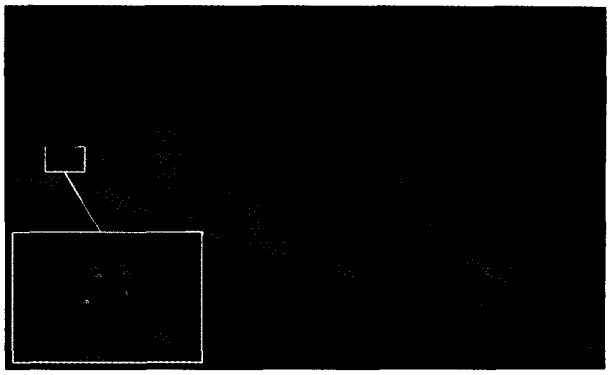

Fig. 4. The vector field topology on the surface of the delta wing. There are a pair of saddle and spiral critical points on each side of the wing (see inset). The integral curves that originate from these points are called closed separation (green) and attachment (red) lines.

simulations, but is difficult in time-accurate simulations because the surface flow patterns can change significantly over time.

3.3 Vector Field Topology

Separation lines can be located using methods based on vector field topology [8], [12]. The topology of a vector field consists of critical points, i.e., points where the velocity is zero, and the tangent curves (instantaneous streamlines) which connect these points. Because the velocity at a critical point is zero, the velocity field in the neighborhood of the critical point is determined by ∇u. Critical points are classified, to a first order approximation, by the eigenvalues and eigenvectors of ∇u. Common classifications include a saddle, node, spiral, and center, as shown in Fig. 6.

In [12], the separation lines were generated by integrating outward from the "saddle" critical points in the real eigenvector directions. These tangent curves, or more precisely, the separatrices, were classified as separation or attachment lines based on the sign of the eigenvalues. That is, a positive or a negative real part of an eigenvalue indicated whether the tangent curve had a repelling or attracting nature, respectively. This approach assumes that the separation is closed, that is, the separation occurs along a line, which begins at a saddle and ends at another critical point. Several closed separation lines are illustrated in Fig. 4. In Section 6, we will demonstrate another type of separation called open separation, which does not obey this condition.

4 Phase Plane Algorithm

An important goal of the present study was to develop a technique to identify and extract separation lines that was consistent with one or more of the current "definitions" discussed in Section 2. We also wanted the technique to be local, meaning that an independent test could be applied to each element on the surface of a body. The phase plane algorithm [14] was the first of two techniques presented. The idea was to model the flow over a simple triangular element and identify the flow patterns that contained streamline asymptotes. Given that the velocity vectors are defined at the vertices, as shown in Fig. 5, a linear vector field can be constructed that passes through the triangle and satisfies the prescribed vectors at the vertices:

$$\begin{pmatrix}\dot{x}\\ \dot{y}\end{pmatrix} = \begin{pmatrix}a_1\\ a_2\end{pmatrix} + \begin{pmatrix}b_1 & c_1\\ b_2 & c_2\end{pmatrix}\begin{pmatrix}x\\ y\end{pmatrix}. \tag{1}$$

Here, (x, y) is the Cartesian coordinate vector and $(\dot{x}, \dot{y})$ the tangential velocity or shear stress vector. For a linear vector field, the coefficients (a_1, a_2) and those in the 2×2 (Jacobian) matrix are constants. These constants can be computed analytically by substituting the coordinates and vectors from each vertex into (1) and then solving the resulting set of simultaneous equations.

By differentiating (1) with respect to time and then algebraically manipulating the resulting equations, one can produce a pair of second order nonhomogeneous ordinary differential equations. The solutions to these types of equations can be found in most texts on differential equations (e.g., [2], [28]). If the determinant of the Jacobian matrix is nonzero, the solution has the form:

$$\begin{pmatrix}x(t) - x_{cp}\\ y(t) - y_{cp}\end{pmatrix} = \begin{pmatrix}\xi_1 & \eta_1\\ \xi_2 & \eta_2\end{pmatrix}\begin{pmatrix}\alpha e^{\lambda t}\\ \beta e^{\mu t}\end{pmatrix}, \tag{2}$$

where λ and μ are the eigenvalues of the Jacobian matrix and (ξ_1, ξ_2) and (η_1, η_2) are the eigenvectors. The two column eigenvectors form the eigenmatrix. The terms α and β are arbitrary constants that define a particular curve in the phase plane. The constants x_{cp} and y_{cp} are the coordinates of the critical point:

$$x_{cp} = \frac{a_2c_1 - a_1c_2}{b_1c_2 - b_2c_1}$$
$$y_{cp} = \frac{a_1b_2 - a_2b_1}{b_1c_2 - b_2c_1} \tag{3}$$

In (2), x_{cp} and y_{cp} translate the coordinate system such that the origin coincides with the critical point. Note that the linear vector field constructed in most triangles will have one critical point. However, that critical point will usually lie outside the boundary of the triangle. The critical points that do lie inside triangles correspond to those found by linear vector field topology methods [11], [12].

Fig. 5. A linear vector field is constructed through one of the triangles (red) on the surface of the delta wing using the shear stress vectors defined at the vertices (blue). The tangent curves (yellow) asymptotically approach the separation line that passes through the triangle.

Using (2), tangent curves can be constructed that pass through the triangle, as illustrated in Fig. 5. In this figure, the tangent curves have been extended beyond the boundaries of the triangle to highlight the asymptote. If we moved along the asymptote toward the front of the delta wing, we would eventually pass through the critical point.

Rather than working in the physical plane of the triangle, we can simplify matters by transforming into canonical coordinates, that is, a coordinate system where the eigenvector directions are orthogonal:

$$\begin{pmatrix} X \\ Y \end{pmatrix} = \begin{pmatrix} \xi_1 & \eta_1 \\ \xi_2 & \eta_2 \end{pmatrix}^{-1} \begin{pmatrix} x(t) - x_{cp} \\ y(t) - y_{cp} \end{pmatrix} = \begin{pmatrix} \alpha e^{\lambda t} \\ \beta e^{\mu t} \end{pmatrix} \tag{4}$$

We have now derived all the equations that are needed to implement the phase plane algorithm. However, we must still establish the conditions under which a streamline asymptote will pass through the triangle and how to calculate the points of intersection. Using (4), the tangent curves of the vector field can be constructed in the (X, Y) plane. This is often referred to as the Poincare *phase plane* [19]. There are five unique portraits for a linear vector field, all of which are shown in Fig. 6.

By eliminating the integration variable, t, from (4), one can express the trajectories of these curves in terms of an implicit scalar function. For the case where both eigenvalues are real numbers, the solution is either:

$$\Psi(X, Y) = \frac{X^{\mu}}{Y^{\lambda}}$$

or

$$\Psi(X, Y) = -\frac{Y^{\lambda}}{X^{\mu}} \tag{5}$$

The contours of $\Psi(X, Y)$ are everywhere tangent to the vector field and may be verified using the relationship $\nabla\Psi \cdot \mathbf{U} = 0$, where $\mathbf{U}$ is the image of the vector field in the phase plane. By differentiating (4) with respect to t, the reader can obtain the necessary transformation, which maps the vector field, $\mathbf{u}$, expressed by (1), into the phase plane. Note that the determinant of the eigenmatrix must equal one so that the vector field is not scaled by the canonical transformation.

$\Psi(X, Y)$ behaves much like Lagrange's stream function for irrotational, divergence free, 2D vector fields inasmuch as the tangent lines are contours of a scalar function. However, $\Psi(X, Y)$ is an exact solution to a rotational 2D linear vector field, which, in general, will not be divergence-free. A nonzero divergence means that mass is not conserved on the surface of the triangle. The fact that this system can *lose mass* is physically important because this accounts for fluid that leaves the surface as the flow converges on a separation line. The system will *gain mass* as the flow returns to the surface and diverges from an attachment line.

One definition of a separation line, discussed in Section 2, is a streamline asymptote onto which adjacent streamlines converge. The phase portrait for the saddle in Fig. 7 contains two such lines. These lines originate at the critical point and are tangential to the eigenvector directions, i.e., the $X = 0$ and $Y = 0$ axes in the phase plane. These lines are called separatrices in phase plane terminology. By substituting either $X = 0$ or $Y = 0$ into (5), we find that the stream function is either zero or singular depending on which solution is used. In either case, these lines do correspond to streamlines and fulfill one of the accepted definitions.

The phase portrait for the improper node can assume one of two orientations in the phase plane depending on whether it is an attracting node ($\mu < \lambda < 0$) or a repelling node ($0 < \mu < \lambda$). Specifically, streamlines asymptotically diverge from the Y-axis for a repelling node, while they converge on the X-axis for an attracting node. Both cases are illustrated Fig. 7. Note that the order of the eigenvalues indicated in Fig. 7 is important because it ensures that the Y-axis is an attachment line, and the X-axis a separation line, in all three portraits.

A separation or attachment line will pass through a triangle if the triangle straddles the X-axis or Y-axis in the phase plane. The vertices of the triangle are mapped into the phase plane using the central expression in (4). The edges of the triangle remain straight because this is a linear transformation. The intersection points are found using linear interpolation along an edge, and then mapped back into the original coordinate system. Implementation details are discussed further in [14].

5 Parallel Vector Algorithm

A technique for locating separation and attachment lines was independently developed from observations made using a 2D vector field topology program called eplane. The eplane program, developed at NASA Ames Research Center in 1989 by Levit [13], allows users to interactively create analytic vector fields ($\mathbf{u}$) with linear, quadratic, and/or cubic polynomial terms. The coefficients of the polynomial can be interactively adjusted using one of 20 sliders. One of the tools in eplane (a data probe) allows the user to visualize the eigenvector directions ($\mathbf{e}_1$ and $\mathbf{e}_2$) of $\nabla\mathbf{u}$ at any point in the field. When the probe was positioned at points where streamlines asymptotically converged, we observed that one of the eigenvectors was always parallel to the local streamlines. That is:

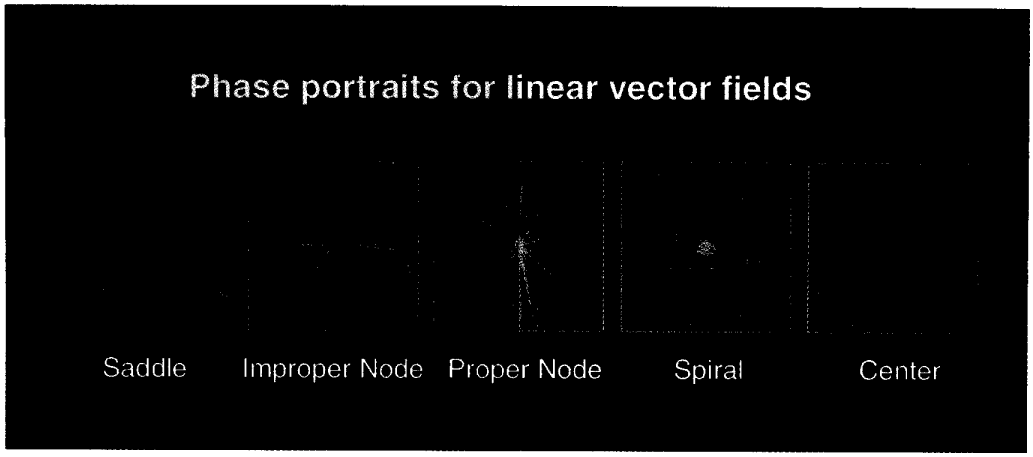

Fig. 6. The five phase portraits for a linear vector field. Only the saddle and improper node contain tangent curves that approach an asymptote.

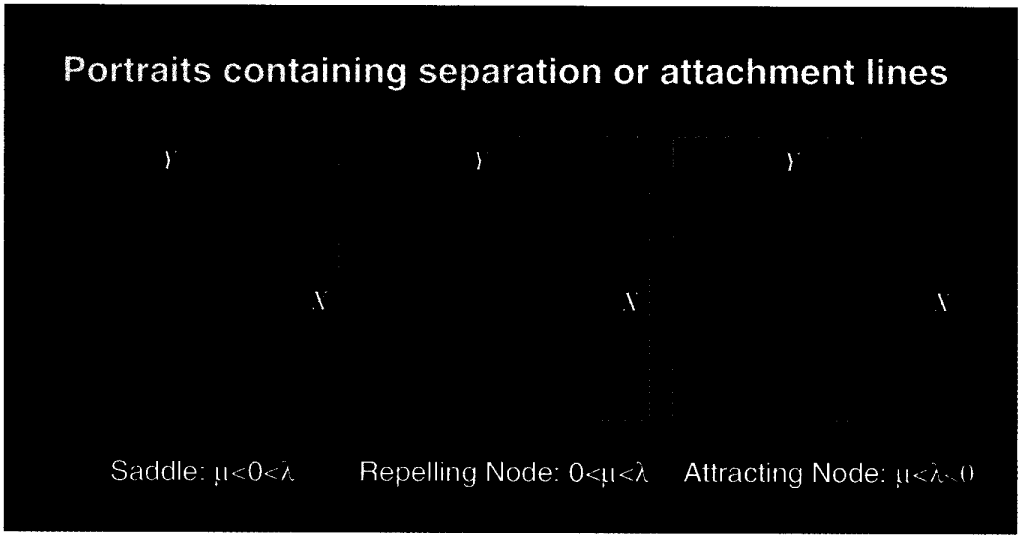

Fig. 7. In the phase plane, a separation or attachment line passes through those triangles that straddle the $X = 0$ or $Y = 0$ axes.

$$\mathbf{e}_i \times \mathbf{u} = 0 \tag{6}$$

This condition also holds true in the phase plane algorithm described in the previous section. That is, the X-axes and Y-axes in Fig. 7 are eigenvector directions, and happen to be the only lines where the eigenvectors are parallel to the velocity vectors. Note that both $\mathbf{e}_1$ and $\mathbf{e}_2$ will be real numbers if a separation or attachment line is present.

The advantage of (6) is that it provides a local test that can be applied at any point in the field. For discrete data, such as those produced by CFD simulations, the velocity vectors and eigenvectors can be evaluated at the vertices and interpolated within the elements. In our implementation for structured grids, the velocity vectors were already defined at the vertices and we calculated $\nabla \mathbf{u}$ at the vertices using central differences. The eigenvectors of $\nabla \mathbf{u}$ were evaluated at the same points.

In the phase plane method, the velocity was piecewise continuous between elements, but the eigenvectors were discontinuous. With the parallel vector method, we can ensure that both the vector and eigenvector directions are continuous between elements by choosing an appropriate interpolation function. A linear interpolation function for $\mathbf{u}$ and $\mathbf{e}_i$ is suitable for triangular elements, while a bilinear function is needed for quadrilateral elements. Because CFD grids usually have a high density of cells near the surface of a body, we found it sufficient to compute the points at which $\mathbf{u}$ and $\mathbf{e}_i$ were parallel on element boundaries.

With the parallel vector method, $\mathbf{e}_i \times \mathbf{u} = 0$ is calculated twice at each vertex, once for the largest eigenvector ($\mathbf{e}_1$) and once for the smallest eigenvector ($\mathbf{e}_2$). Note that this test is only applied if the eigenvalues are both real, i.e., the classification of $\nabla \mathbf{u}$ at the vertex is a saddle or a node. If $\mathbf{e}_i \times \mathbf{u}$ changes sign across an edge, then a separation line or attachment line will intersect the edge. The intersection point is calculated by linearly interpolating the cross product across an edge. It is easy to distinguish the separation and attachment lines since the separation lines occur where $\mathbf{e}_1 \times \mathbf{u} = 0$ and attachment lines occur where $\mathbf{e}_2 \times \mathbf{u} = 0$. A continuous line can be constructed by connecting the respective points in each element.

After testing the algorithm, we found that (6) was necessary but not sufficient for extracting separation lines. In particular, it detects an extra set of lines that are the locus of inflection points in the vector field. These are called inflection lines hereafter. The flow pattern that gives rise to inflection lines is shown in Fig. 8. Along inflection lines, one of the eigenvectors is locally parallel to the velocity vector, but the inflection line itself is not an asymptote of neighboring streamlines. This was first reported by Wu et al. [26]. Inflection lines are interesting from a topological viewpoint, but they are not usually significant to aerodynamicists. Consequently, we filter these lines out using directional derivative test.

For a separation line, defined by (6), to be a streamline, the quantity $\mathbf{e}_i \times \mathbf{u}$ must remain zero along the streamline. This condition, that $\mathbf{e}_i \times \mathbf{u} = 0$ is a constant of the motion, is true locally iff:

$$\mathbf{e}_i \times \mathbf{u} = 0 \quad \text{and} \quad \nabla(\mathbf{e}_i \times \mathbf{u}) \cdot \mathbf{u} = 0 \tag{7}$$

Equation (7) is the directional derivative test. Along inflection lines, $\mathbf{e}_i \times \mathbf{u} = 0$, but $\nabla(\mathbf{e}_i \times \mathbf{u}) \cdot \mathbf{u} \neq 0$. We use a numerical version of the integral form of these expressions to reject inflection lines.

6 Results

The phase plane and parallel field algorithms were applied to analytic 2D vector fields generated by the eplane topology program [13] as well as to results from CFD simulations [4]. In this study, we examined a large number of analytic vector fields with successively higher-order polynomial terms. The four analytic vector fields presented here were chosen because they highlight some of the strengths and weaknesses of the two approaches.

6.1 Linear Vector Fields

Fig. 9a and 9b show two linear vector fields, a saddle and a node, that were generated from (8) and (9):

$$\textit{Saddle:} \quad u = x, \quad v = x + y \tag{8}$$

$$\text{Node:} \quad u = x + y, \quad v = 2y \tag{9}$$

Because both the phase plane and parallel field algorithms are based on linear interpolation functions, they produce exact and identical results for linear vector fields. Two such fields are shown in Fig. 9. The point at which the separation (green) and attachment lines (red) intersect is a critical point (zero velocity). The separation and attachment lines are always straight lines in linear vector fields (with two real eigenvalues) and are always parallel to the eigenvector directions. Note that the tangent curves (black) asymptotically approach both axes of the saddle, whereas there is a predominant axis of attraction (or repulsion) for the node.

Although the direction of flow is not indicated on the tangent curves, it can easily be deduced from the color coding. That is, the flow moves toward a separation line, while it moves away from an attachment line. This seems counterintuitive until you consider what happens in three dimensions. Separation occurs where two opposing flow directions meet and are forced to lift off a solid body. The flow must, therefore, approach a separation line in order for this to occur.

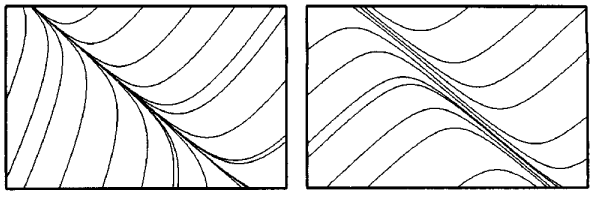

Fig. 8. The vector field on the left contains a separation line whereas the field on the right contains an inflection line.

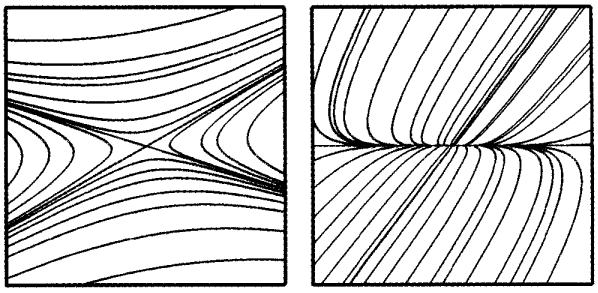

Fig. 9. The separation (green) and attachment lines (red) were accurately located by both phase plane and parallel field algorithms in these simple analytic test cases: (a) saddle and (b) node.

6.2 Open Separation

The second analytic test case is a vector field with quadratic terms:

$$u = \frac{1}{2}\left(x^2 + 2xy + y^2\right),$$

$$v = \frac{1}{2}\left(-1 + x^2 + 2xy + y^2\right) \tag{10}$$

This vector field, illustrated in Fig. 10, is interesting because it has no critical points anywhere, but it still contains separation and attachment lines. These are open separation and attachment lines according to Chapman [5] because they neither start or end at a critical point. Topology-based methods, such as those described in [6], [7], [11], [12], will not detect this type of separation line. This example of open separation is not an isolated case. We were able to create several analytic vector fields using eplane that contained open separation lines. These lines may be straight or curved.

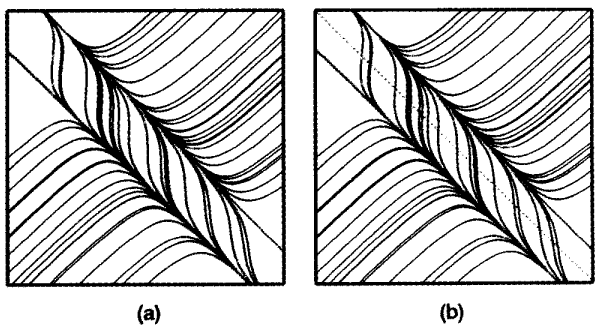

Fig. 10. An analytic vector field that contains two open separation and attachment lines. These were extracted using: (a) the phase plane and (b) the parallel field algorithms.

This vector field holds particular interest because parallel separation and attachment lines with this flow pattern frequently occur on delta wing aircraft. The separation and attachment lines in Fig. 10a were produced by the phase plane algorithm and those in Fig. 10b by the parallel field. Both algorithms successfully identified the limiting lines in this vector field. The disconnected points that lie inbetween the separation and attachment lines are inflection points on the streamlines. These points were rejected by the directional derivative test. Note that the locus of points, i.e., the inflection line, is not an asymptotic streamline and is not, therefore, a separation line. Even in CFD data sets, an inflection line will usually exist between a separation and attachment line, so it is necessary that it be removed with the directional derivative test.

6.3 Three-Way Symmetry

The third analytic vector field, illustrated in Fig. 11, contains a number of critical points including a higher-order critical point called a monkey saddle. This vector field was created using the equations:

$$u = x + x^2 - y^2, \quad v = y - 2xy \tag{11}$$

Note that the flow diverges much faster from the attachment lines (red) than it converges on the separation lines (green). This indicates that the flow is moving much faster along the separation lines. In a real flow, where fluid can leave the two-dimensional plane, slowly converging streamlines indicate that separation (or attachment) is relatively weak. The disparity between the strength of the separation and attachment highlights a difference between the phase plane and parallel field algorithms. Compare the results in Fig. 11a and 11b. The phase plane algorithm produces many false positives, i.e., additional line segments, along the weak separation lines.

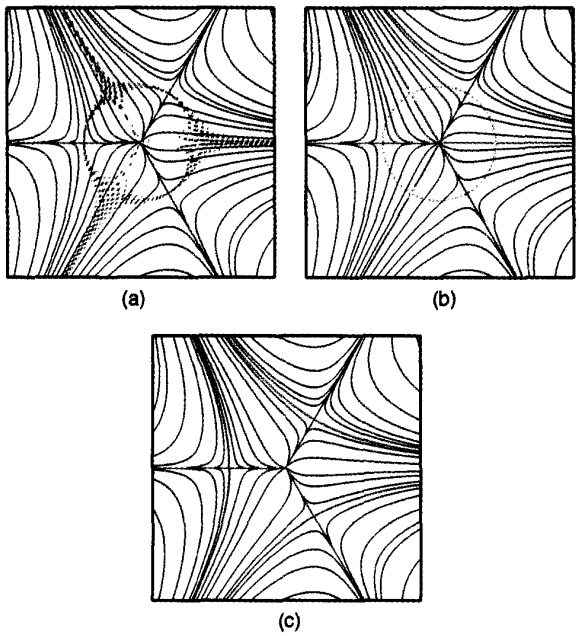

Fig. 11. An analytic vector field that contains a higher-order critical point known as a monkey saddle. The separation and attachment lines were extracted using the a) phase-plane, (b) parallel field, and (c) vector field topology algorithms.

This is because the eigenvectors are constant over each element [14]. The parallel vector method does not suffer this problem because both the velocity and the eigenvectors are piecewise linear.

The circle of dots in Fig. 11b is the inflection points, where the streamline curvature is zero. As noted before, these can be eliminated with the directional derivative test. They are shown here only for illustration. Fig. 11c shows the vector field topology computed by eplane. The tangent curves were integrated in the direction of the real eigenvectors from each of the three saddle points. The topology algorithm in eplane only detects linear critical points, which accounts for the missing separation lines that originate from the monkey saddle in Fig. 11c. A higher-order critical point algorithm [20] is needed to locate these lines.

6.4 Curved Separation Lines

The linear methods described in this paper do not always detect separation or attachment lines that are curved. Compare the vector fields for the monkey saddle in Fig. 11b and 11c. The topology algorithm finds three curved separation lines that are not detected by the phase plane or parallel vector algorithms. These originate at the saddle points on the circular inflection line.

The underlying problem became apparent when we studied the curved saddle shown in Fig. 12. The generating equation was similar to (8) with the addition of a quadratic term.

Both the phase plane and parallel vector algorithms detect points where the curvature is locally zero. In Fig. 12, the separation and attachment lines both diverge from the asymptotic streamline because it has nonzero curvature. The lines turn into points when the directional derivative test fails. The (predicted) attachment line diverges slower because the attaching flow is stronger and the locus of zero curvature points lies closer to the asymptotic streamline. This appears to be a serious limitation of the linear algorithms. However, results presented in the next section will show that, even in complicated vector fields resulting from CFD simulations, the assumption that the flow is locally linear is usually satisfactory.

6.5 Delta Wing

The delta wing platform is used in many fighter aircraft because it has many desirable aerodynamic and structural qualities. Aeronautical engineers are particularly interested

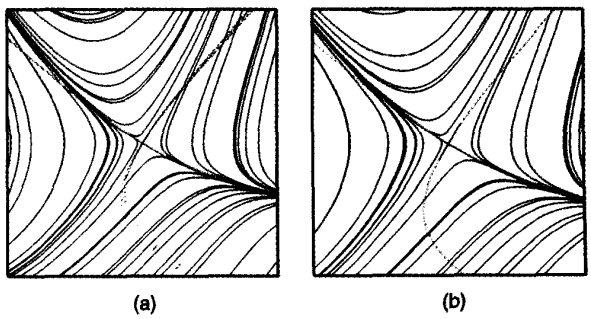

Fig. 12. The phase plane and parallel vector algorithms are based on locally linear interpolants of the vector field. Curved separation lines pose a problem.

Fig. 13. Vector arrows rendered on a cutting plane reveal the vortices above the delta wing. The flow detaches from the surface along a separation line (green) and returns along an attachment line (red).

in the behavior of the flow both on and above the wing while flying at low speeds and high angles of attack [4]. The skin friction lines, shown previously in Fig. 2, reveal many asymptotically converging streamline patterns along the leading edges of the wing. Chaderjian and Schiff [4] used skin friction lines to analyze the surface flow on a delta wing and reported the following: "The technique clearly reveals the separation lines where particles accumulate. Reattachment lines are not as readily apparent, since on attachment lines the particles move away from each other. However, computed primary, secondary and tertiary separation lines are readily seen."

The separation lines that Chaderjian and Schiff discuss are linked to the vortical flow above the wing. Rendering vector arrows on a transverse plane can reveal this flow, as illustrated in Fig. 13. The primary and secondary vortices are clearly visible in this figure, but the tertiary vortex, which lies in between them, is less obvious because it hugs the surface. Each vortex draws fluid off the surface along separation lines and returns fluid to the surface along attachment lines. Consequently, the latter are often called reattachment lines. Given that each vortex is both drawing fluid and returning it to the surface, we expect to see an equal number of separation and attachment lines.

The vector field topology of the delta wing was computed using a topology module in FAST [11]. Surprisingly, only two pairs of critical points were found on the surface of the wing. Those on the right wing are shown in the inset in Fig. 4. The critical points on the left wing are mirror images of those on the right wing. A more comprehensive critical point analysis of the entire 3D flow field revealed that there were no off-surface critical points at all in this data set. Each pair of critical points consists of one repelling spiral point and one saddle point. Note that only one of the integral curves that originates from each saddle point follows an attachment line. None of the other primary, secondary, or tertiary separation or attachment lines either start or end at one of the two critical points. These are open separation and attachment lines according to Chapman [5] and Wang et al. [24], [25]. Flow topology methods cannot detect this type of open separation line because they are not bounded by any critical points, either on or off the body.

The phase plane algorithm extracted all of the primary, secondary, and tertiary separation (green) and attachment lines (red) from this data set. The results are shown in Fig. 14. There are three separation lines and three attachment lines on each side of the wing, that is, one pair for each vortex. Furthermore, their location precisely coincides with the asymptotes of the streamlines.

Note the disjointed line segments near the center of the wing where the attaching flow is relatively weak and diffused over several elements. This behavior is a consequence of the linear interpolation function on which the phase plane algorithm is based. The location and direction of an attachment (or separation) line is dictated by the gradients of the interpolation function. For the phase plane algorithm, these gradients are constant over each triangle but discontinuous between triangles. This discontinuity becomes apparent when the separating or attaching flow is weak. In the delta wing data set, the weak attachment lines were less important from an engineering standpoint and the phase plane algorithm produced acceptable results.

The separation and attachment lines extracted by the parallel field algorithm are shown in Fig. 15. All inflection lines have been removed for clarity. The line connectivity produced by the parallel field algorithm is superior to the

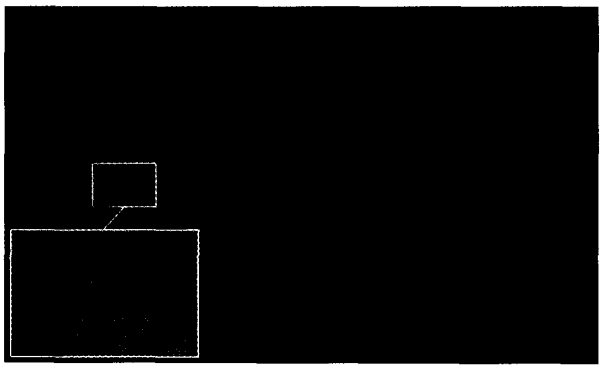

Fig. 14. Separation and attachment lines extracted by the phase plane algorithm. All the important lines are identified, although the low-order interpolant produces some visually distracting artifacts near the center of the wing where the attaching flow is weak.

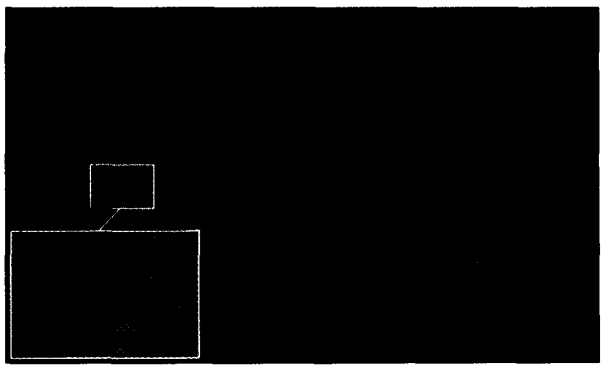

Fig. 15. The parallel vector algorithm also extracts the primary, secondary, and tertiary separation and attachment lines. The line connectivity is better because both the velocity and eigenvector fields are piecewise continuous in this algorithm.

phase plane algorithm because the velocity vectors and eigenvectors are continuously interpolated across element boundaries. This guarantees that a separation or attachment line will have a common intersection point on the shared edge between neighboring elements.

Most of the separation and attachment lines in Figs. 14 and 15 are the open type, which do not start or end at critical points [5], [24], [25]. All of the separation and attachment lines in this flow have very little curvature, so the problem identified in Section 6.4 had no significant effect in this data set. However, this may not always be true. Higher-order versions of the algorithms described here are required to accurately extract curved separation and attachment lines.

7 Analysis

Two important benefits of feature extraction algorithms are time and data reduction. These were quantified for each of the feature detection algorithms discussed in this paper. The surface of the delta wing aircraft was comprised of 9,823 quadriateral elements in a structured curvilinear mesh. Each quadrilateral was subdivided into two triangles for the phase plane algorithm. On an SGI Onyx 2 with one 195 MHz R10000 CPU, the feature extraction took 0.73 sec for the phase plane algorithm and 0.90 sec for the parallel vector algorithm.

The delta wing data set originally consisted of an 8.2 MB mesh file and a 13.7 MB solution file. The amount of geometry (3D line segments) produced by the feature extraction algorithms was 66 KB for the phase plane algorithm and 45 KB for the parallel vector algorithm. The output geometry was, therefore, several hundred times smaller than the input data. In general, the data reduction offered by these techniques will improve on larger data sets because the number of surface elements increase as a square of the grid dimensions, whereas the number of volume elements increase as a cube of the grid dimensions.

The results presented in Section 6 indicated that the parallel vector algorithm was slightly superior to the phase plane algorithm. However, implementation issues must also be considered. The phase plane algorithm is well-suited to unstructured meshes because the analysis is self-contained within each triangle. The parallel vector algorithm is harder to implement because the vector gradients are difficult to calculate on irregular triangulations. For curvilinear meshes, the parallel vector algorithm is the best choice because the vector gradients can be readily calculated using central differences. It also solves the line discontinuity problem that was inherent in the phase plane algorithm.

8 Conclusion

Two algorithms have been presented that identify and extract separation and attachment lines on 2D surfaces in 3D vector fields. Both algorithms use eigenvector analysis of the velocity gradient tensor to identify these lines. The first technique (the "phase plane" algorithm) is element-based and detects streamline asymptotes using local linear approximations on triangles. The second approach (the "parallel vector" algorithm) is point-based and detects places where the velocity vectors are parallel the eigenvectors, i.e., points where the streamline curvature is zero. This condition also identifies inflection lines, although these can be removed using a directional derivative test. Both approaches correctly identify separation and attachment lines in many analytic test cases, although they may fail in vector fields with curved separation lines. The parallel vector algorithm generally produces slightly better visualizations than the phase plane algorithm because it ensures global continuity of the velocity and eigenvector fields. Of particular significance, both approaches detect open separation lines, that is, separation lines that do not start or end at critical points. Traditional topology algorithms do not capture open separation lines because they trace separation lines by integrating along the insets and outsets of saddle points.

Acknowledgments

This work was supported by the National Aaeronautics and Space Administration under Contract NAS2-14303. The authors wish to thank Neal Chaderjian for providing the delta wing data set and David Kao for generating the LIC textures. special thanks to Tim Sandstrom and Han-Wei Shen for assistance with the VisTech Library and Pat Moran for assistance with the Field Encapsulation Library.

References

[1] R.F.W. Bader, *Atoms in Molecules—A Quantum Theory*. Oxford, U.K.: Oxford Univ. Press, 1990.
[2] F. Brauer and J.A. Nohel, *Qualitative Theory of Ordinary Differential Equations*. W.A. Benjamin, Inc., pp. 33-95, 1969.
[3] B. Cabral and C. Leedom, "Imaging Vector Fields Using Line Integral Convolution," *Proc. Computer Graphics, ACM SIGGRAPH*, pp. 263-270, 1993.
[4] N.M. Chaderjian and L.B. Schiff, "Navier-Stokes Analysis of a Delta Wing in Static and Dynamic Roll," AIAA-95-1868, AIAA Ann. CFD Meeting, 1995.
[5] G.T. Chapman, "Topological Classification of Flow Separation on Three-Dimensional Bodies," AIAA-86-0485, AIAA 24th Aerospace Sciences Meeting, Reno, Nev., 1986.
[6] M.S. Chong, A.E. Perry, and B.J. Cantwell, "A General Classification of Three-Dimensional Flow Fields," *Physical Fluids A.*, vol. 2, pp. 765-777, 1990.
[7] M.S. Chong and A.E. Perry, "Synthesis of Two- and Three-Dimensional Separation Bubbles," *Proc. Ninth Australasian Fluid Mechanics Conf.*, pp. 35-38, Auckland, New Zealand, Dec. 1986.
[8] U. Dallman, "Topological Structures of Three-Dimensional Vortex Flow Separation," AIAA-83-1935, *Proc. AIAA 16th Fluid and Plasma Dynamics Conf.*, 1983.
[9] W.C. de Leuuw, H.-G. Pagendarm, F.H. Post, and B. Walter, "Visual Simulation of Experimental Oil-Flow Visualization by Spot Noise Images from Numerical Simulation," *Visualization in Scientific Computing '95*, pp. 135-148, Wien, Springer-Verlag, 1995.
[10] L.K. Forssell, "Visualizing Flow Over Curvilinear Grid Surfaces Using Line Integral Convolution," *Proc. IEEE Visualization '94*, pp. 240-247, 1994.
[11] A. Globus, C. Levit, and T. Lasinski, "A Tool for Visualizing the Topology of Three-Dimensional Vector Fields," *Proc. Visualization '91*, pp. 33-40, 1991.
[12] J.L. Helman and L. Hesselink, "Surface Representations of Two- and Three-Dimensional Fluid Flow Topology," *Proc. Visualization '90*, pp. 6-13, 1990.
[13] C. Levit, *Conf. Scientific Applications of the Connection Machine*, NASA Ames Research Center, Moffett Field, Calif., Sept. 1989.
[14] D.N. Kenwright, "Automatic Detection of Open and Closed Separation and Attachment Lines," *Proc. IEEE Visualization '98*, pp. 151-158, 1998.

[15] M.J. Lighthill, "Attachment and Separation in Three-Dimensional Flow" *Laminar Boundary Layers*, L. Rosenhead II, ed., vol. 2.6, pp. 72-82, Oxford Univ. Press, 1963.
[16] W. Merzkirch, *Flow Visualization*. New York: Academic Press, 1974.
[17] H.-G. Pagendarm and B. Walter, "Feature Detection from Vector Quantities in a Numerically Simulated Hypersonic Flow Field in Combination with Experimental Flow Visualization," *Proc. Visualization '94*, pp. 117-123, 1994.
[18] R.L. Panton, *Incompressible Flow*. John Wiley & Sons, 1984.
[19] H. Poincare, *Oeuvres de Henri Poincare*, Tome 1. Paris: Gautheir-Villars, 1928.
[20] G. Scheuermann, H. Hagen, H. Kruger, M. Menzel, and A. Rockwood, "Visualization of Higher Order Singularities in Vector Fields," *Proc. IEEE Visualization '97*, pp. 67-74, 1997.
[21] H. Shen and D.L. Kao, "UFLIC: A Line Integral Convolution Algorithm for Visualizing Unsteady Flows," *Proc. IEEE Visualization '97*, pp. 317-322, 1997.
[22] M. Tobak and D.J. Peake, "Topology of Three-Dimensional Separated Flows," *Ann. Review of Fluid Mechanics*, vol. 14, pp. 61-85, 1982.
[23] J.J. van Wijk, "Spot Noise: Texture Synthesis for Data Visualization," *Computer Graphics*, vol. 25, no. 4, pp. 309-318, 1991.
[24] K.C. Wang, "Separation Patterns of a Boundary Layer Over an Inclined Body," *AIAA J.*, vol. 10, no. 8, pp. 1,044-1,050, 1972.
[25] K.C. Wang, H.C. Zhou, C.H. Hu, and S. Harrington, "Three-Dimensional Separated Flow Structure Over Prolate Spheroids," *Proc. R. Soc. London*, A 421, pp. 73-90, 1990.
[26] J.Z. Wu, J.W. Gu, and J.M. Wu, "Steady Three-Dimensional Fluid Particle Separation from Arbitrary Smooth Surface and Formation of Free Vortex Layers," AIAA-87-2348, AIAA Ann. CFD Meeting, 1987.
[27] H.X. Zhang, *Chinese J. of Aerodynamics*, no. 4, Beijing, Peoples Republic of China, Dec. 1985.
[28] D. Zwillinger, *Handbook of Differential Equations*, second ed. Academic Press, pp. 360-363, 1957.

David N. Kenwright received his BE degree (with first class honors) in 1988 and his PhD degree in mechanical engineering in 1994, both from the University of Auckland, New Zealand. Dr. Kenwright is a senior research scientist with MRJ Technology Solutions, Inc., and works in the Data Analysis Group at NASA Ames Research Center. His current research interests include flow feature detection and biomimetics. He is a member of the IEEE, IEEE Computer Society, and AIAA.

Chris Henze received his PhD degree in ecology and evolutionary biology from the University of Arizona in 1993. He is employed by MRJ Technology Solutions, Inc., and is currently a research scientist in the Data Analysis Group at the Numerical Aerospace Simulation facility at NASA Ames Research Center. His primary research interests include vector field topology, flow visualization, computational chemistry, and molecular phylogenetic systematics.

Creon Levit has been employed at NASA Ames research center since 1982. He has worked as a research scientist in scientific visualization, computational fluid dynamics, and molecular physics since 1988.